Title
THE CRYOGENIC MECHANICAL PROPERTIES OF HIGH MANGANESE AUSTENITC STAINLESS STEELS

Author
Morris, J.W.

Publication Date
1986-07-01

LBL-21933
Preprint

Submitted to Metallurgical
Transactions A

THE CRYOGENIC MECHANICAL PROPERTIES OF HIGH MANGANESE AUSTENITC STAINLESS STEELS

R. Ogawa and J.W. Morris, Jr.

July 1986

cam

Lawrence Berkeley Laboratory
University of California
Berkeley, California 94720

Center for Advanced Materials

Prepared for the U.S. Department of Energy under Contract DE-AC03-76SF00098

DISCLAIMER

THE CRYOGENIC MECHANICAL PROPERTIES OF

HIGH MANGANESE AUSTENITC STAINLESS STEELS

R. Ogawa* and J.W. Morris, Jr.

Department of Materials Science and Mineral Engineering
and
Lawrence Berkeley Laboratory
University of California, Berkeley 94720

ABSTRACT

The potential of high manganese stainless steel as a new high strength cryogenic steel was investigated over a wide range of alloy compositions. The alloys containing delta ferrite showed a pronounced loss of toughness after solution treatment plus aging because of the transformation of delta ferrite to a brittle sigma phase. Manganese behaves as a ferrite stabilizing element in the Fe-Mn-Ni-Cr-N system. Alloys containing carbon also showed a loss of toughness after solution treatment plus aging due to the grain boundary precipitates of $M_{23}C_6$ carbide. A stable alloy of nominal chemical composition 18Mn-5Ni-16Cr-0.02C-0.22N is shown to have an excellent combination of strength and toughness at cryogenic temperature.

* Now at the Materials Research Laboratory, Kobe Steel Ltd., Japan

I. INTRODUCTION

Nitrogen strengthened austenitic stainless steels, AISI 304LN and 316LN, have been used as high strength structural materials for recently constructed large superconducting magnets. Both steels contain about 0.10 -0.15% nitrogen and have been reported to have the yield strength in the range of 800-1000 MPa at 4 K together with a fracture toughness (K_{IC}) of around 200 MPa $\sqrt{m}$ [1]. Although both steels have almost twice the yield strength at 4 K of 304L and 316L steel, their strengths are not still sufficient to satisfy requirements for high field superconducting magnets for fusion reactor use. In order to satisfy this need, several types of high manganese steels have been investigated. The steels, 25Mn-5Cr-2Ni [2], 32 Mn-7Cr-1Ni [3] and 30 Mn-5A [4], are reported to have high strength and toughness at 4.2 K. However, their strength levels are no more than comparable to those of 304LN and 316LN steels. High manganese steels, however, offer the advantage of replacing the more expensive nickel that is present in 304LN and 316LN. Manganese stabilizes the austenite phase and increases the solubility of nitrogen which permits the achievement of higher strength. The high manganese and high chromium steels containing nitrogen and little nickel are standardized as the AISI 200 series Mn-Cr stainless steels. These steels have high yield strength (more than 1300 MPa) but show poor ductility at 4.2 K [5].

The influence of alloy composition on the ductility and the toughness of the Mn-Cr stainless steels was investigated in an attempt to improve their cryogenic properties. One alloy was selected after preliminary tests, and its fracture toughness was investigated at 4.2 K.

II. EXPERIMENTAL PROCEDURE

Ten kilogram ingots of Fe-Mn-Cr-Ni-N-C alloys were prepared by vacuum induction melting. The chemical compositions of the ingots are given in Table I. The base alloy is a modified AISI 205 alloy with nominal composition 18Mn-5Ni-16Cr-0.03C-0.26N (Alloy A). The influence of Mn was investigated for the alloys containing 5% Ni and 1% Ni. The carbon content was also varied from 0.03% to 0.16% holding the carbon plus nitrogen content at the constant value of 0.28%. The influence of Cr and Ni were investigated in the range of 12-18% and 1-7%, respectively.

All ingots were forged to 50 mm thickness plates and then hot rolled to 15 mm thickness after holding for 1 hr at 1100^{o}C. The plates were subsequently solution-treated for 30 min at 1050^{o}C followed by quenching in water. Some plates were aged for 45 min at 660^{o}C after solution treatment. Charpy impact properties were measured at 77 K, using a 2 mm V-notched Charpy specimen. The alloys were tested in three conditions: as hot rolled, solution treated (1050^{o}C for 30 min + water quenching) and aged (660^{o}C for 45 min + air cooling) after solution treatment. Tensile tests were performed at 77 K and 4.2 K. The tensile test at 4.2 K was done in a multi-specimen tensile cryostat [6] in which twelve specimens can be set. All specimens were prepared in the rolling direction of the plates. The parallel part of the specimen was 3.0 mm x 20 mm . The tensile tests were performed at a cross-head speed of 0.5 mm/min ($4 \times 10^{-4} S^{-1}$). Auger electron spectroscopy measurements were made on the fractured surfaces of brittle specimens.

After these preliminary tests, one alloy was selected. A 300 kg ingot was prepared by vacuum melting and forged to 80 mm thickness plates. The chemical compositions of the plates are given in Table 2. The forged plates were hot rolled to 30 mm thickness in three conditions of different soaking temperatures, 1250, 1200 and 1150°C for one hour. A part of the plate hot rolled at 1200°C was reheated at 1050°C for 30 min followed by quenching in water. Tensile and compact tension specimens were obtained in the rolling direction of the plate. In this case, tensile tests at 4.2 K were done in a single specimen tensile cryostat at a cross-head speed of 0.5 mm/min. The parallel part of the test specimen was 6/35 mm x 38.1 mm .

Fracture toughness measurements were made on a one-inch compact tension specimen (B=25.4 mm, W=50.8 mm). J-resistance curves were obtained at 4.2 K by using the crack length versus unloading compliance correlation. J_{IC} value was taken at the intersection of the J-integral curve with the blunting line, and $K_{IC}(J)$ was obtained by the following equation:

$$K_{IC}(J) = \frac{E \cdot J_{IC}}{1 - \upsilon^2}$$

where E is Young's modulus and υ is Poisson's ratio.

III. RESULTS AND DISCUSSION

A. The Influence of Mn, Cr and Ni on the Tensile Properties and the Charpy Impact Toughness.

The influence of the substitutional species (Mn, Cr and Ni) on the tensile properties at 4.2 K are presented in Figs. 1-4. Figures 1 and 2 show the influence of Mn on the tensile properties of 5% Ni and 1% Ni alloys, respectively. In 5% Ni alloys, the yield strength increases as the Mn content increases from 15% to 18%. The tensile strength and the elongation have the almost constant values for the Mn range tested. The low yield strength and the high work-hardening rate of the 15% Mn alloy may be due to the less stable austenite phase, because about 60% ε phase and 15% α phase were detected in a specimen fractured at 4.2 K. The yield strength of 1% Ni alloys also increases with increasing Mn content. Relatively low elongation was obtained in the 18% Mn alloy and the 29% Mn alloy. Figures 3 and 4 show the influence of Cr and Ni, respectively. The alloys containing 12% to 18% Cr have almost identical tensile properties. The alloys containing low Ni have uniformly lower elongation than those with 5 Ni. No further improvement is seen on increasing the Ni content from 5% to 7%.

The influence of the substitutional species, (Mn, Cr and Ni) on the Charpy V-notch impact energy at 77 K is shown in Figures 5 and 6. Figure 5 shows the influence of Mn on the Charpy impact values of the alloys containing 5% Ni and 1% Ni. The impact values of 5% Ni alloys are greater than those of 1% Ni alloys, and the impact value in the as-rolled condition decreases gradually with an increase in the Mn content. The solution treatment improves the toughness remarkably. Since the yield strength of the as-hot-rolled alloys ranged from 1000-1300 MPa at 77 K and decreased to 800-1000 MPa after solution treatment, the improvement in toughness is mainly attributed to the decrease in the yield strength. In several alloys the Charpy impact values decrease rapidly after solution treatment plus aging. This result indicates that some precipitation in the present alloy system deteriorates the toughness remarkably. The decrease in the Charpy impact value after solution treatment plus aging is observed in three 1% Ni alloys and 5% Ni alloys containing 29% Mn.

Figures 6a and 6b show the influence of Ni and Cr on the Charpy impact values. The deterioration of the toughness by aging is observed in the low Ni content alloy (1% Ni alloy) and the high Cr content alloy (18% Cr alloy).

All of the alloys that lost toughness on aging were found to include delta ferrite by the optical microscopic observations and permeability measurements. The results of permeability measurements with a simple μ-meter and a magnegauge are summarized in Table 3. The alloys listed in Table 3 show permeabilities of more than 1.02 after solution treatment ($1050^{\circ}C$ x 30 min -> WQ). The alloys containing 1% Ni show the increasing permeability with increasing Mn content. The 29%Mn-1%Ni-16%C has a ferrite number of 4.6. The delta ferrite content increases with increasing Mn and Cr and decreasing Ni content. After solution treatment plus aging at $660^{\circ}C$ for 45 min, all of the alloys exhibit a very low permeability, less than 1.01, as shown in Table 2. This suggests that the delta ferrite transforms to a non-magnetic phase on aging. The new phase was identified as a sigma phase by an electron diffraction analysis. The deterioration of the toughness observed in the alloys containing delta ferrite after solution treatment plus aging is therefore attributed to the transformation of delta ferrite to a brittle sigma phase. The fracture surfaces after solution treatment plus aging are shown in Fig. 7. Figure 8 shows the optical micrographs of the 29Mn-1Ni-16Cr steel after solution treatment (a) and solution treatment plus aging (b). There is no large change in the delta-ferrite morphologies between the two conditions.

Omori, et al. [7] reported that delta ferrite in dual-phase stainless steels decomposes to sigma phase and austenite by eutectic decompostion after carbide precipitates at the grain boundary between delta ferrite and austenite. Figure 9 shows an example of a sigma-phase particle in 18Mn-1Ni-16Cr steel after solution treatment plus aging. No eutectic constituent is visible. The decomposition of the delta phase has been reported to need a relatively long incubation time at around $650^{\circ}C$ if the carbon content is low. On the other hand, in the Fe-Mn-Cr-Ni system of the present alloy, the incubation time seems to be very short, and delta ferrite transforms completely to sigma phase in a short time. Table 4 shows the chemical compositions of the phases present in 29Mn-1Ni-16Cr steel in the two conditions. Chromium is enriched in delta ferrite and sigma phase. Other elements (Mn, Fe and Ni) are depleted in both phases. The concentrations of the main elements are almost the same in both delta and sigma phases. This implies that the transformation does not require a large concentration change. The chemical equation of the sigma phase of the present alloy is found to be $(Cr_{12}Mn_{13})(FeNi)_{25}$, and the valence electron per atom ratio (e/a) is 7.27. The valence electron per atom ratios (e/a) of the sigma phases in chromium-nickel austenitic steels has been reported [8] to lie between 7.22-7.96, and the composition of the sigma phase in 25Cr-20Ni steels is expressed by the chemical formula $Cr_{23}Fe_{23}Ni_{4}$.

The existance region for the delta ferrite is shown in Fig. 10. The boundary of delta ferrite formation was estimated as shown in Fig. 10. The boundary shifts to lower Mn and Cr contents with a decrease in Ni content. The Shoefler [9] and DeLong [10] diagrams for delta ferrite in the Fe-Ni-Cr system are plotted using Ni and Cr equivalencies. The delta ferrite content increases with increasing Cr equivalence and decreases with increasing Ni equivalence. In both the Shoefler and DeLong diagrams, manganese is included in the Ni equivalence as an austenite stabilizing element. However, manganese in the present Fe-Mn-Cr-Ni system behaves like chromium.

Henry, et al. [11] have reported the same kind of behavior of manganese. Hull [12] has pointed out the inversion behavior of manganese from an austenitic to a ferrite-stabilizer at manganese levels above 4% in Fe-Ni-Cr alloys. However, his diagram could not be applied to the present alloy system. This discrepancy may be due to the difference of the alloy composition between the present high manganese alloy system and Hull's alloy system.

B. The Influence of Carbon on Strength and Charpy Impact Toughness.

The influence of carbon substitution for nitrogen on the tensile properties of 18Mn-5Ni-16Cr steels at 4.2 K is presented in Fig. 11. Yield and tensile strengths of the alloy in its three conditions (as rolled, solution treated, solution treated plus aging) decrease with increasing carbon content. Since the carbon plus nitrogen content is kept almost constant in these alloys, nitrogen is more effective in raising the strength than carbon. The different contribution to the strength of carbon and nitrogen has been reported in 304 steel by Takahashi, et al. [13]. The alloys containing 0.10% and 0.16% carbon show a decrease in total elongation on aging at 660°C for 45 min after solution treatment.

The influence of carbon on the Charpy impact values at 77 K is given in Fig. 12. The alloys containing 0.10% and 0.16% C again show a loss of toughness after solution treatment plus aging. As these alloys do not contain delta ferrite, the deterioration of the toughness may be due to the precipitation of a carbide. Figure 13 shows the fracture surface of the notched specimen fractured by a hammer at 77 K in the specimen chamber of an Auger electron spectroscope (AES). Intergranular facets are included in primarily ductile dimple fracture, and the grain boundary facets comprise fine small dimples which correspond to fine precipitation on the grain boundary. Auger spectra taken from the grain boundary facets indicated segregation of carbon.

Grain boundary precipitates are clearly visible in Fig. 14 and were identified as $M_{23}C_{6}$ carbide by selected-area electron diffraction. These precipitates evidently cause the deterioration of the toughness during aging. Therefore, the carbon content should be lowered, and the alloys should be strengthened by the addition of nitrogen.

C. Selection of a New High Strength Cryogenic Steel.

These preliminary tests identify a suitable range for a new high strength cryogenic steel. First, alloys containing delta ferrite show a pronounced loss of toughness after solution treatment plus aging. Delta ferrites are formed in the alloy having a high manganese, high chromium, or low nickel content. The boundary of the delta ferrite region in the Fe-Ni-Cr system shifts to the high manganese and high chromium side with increasing nickel content. Since the delta ferrite transforms to a brittle sigma phase by aging and reduces the toughness remarkably, the formation of the delta ferrite must be avoided in the cryogenic steel. The minimum Cr content is fixed by the need for corrosion resistance. High manganese steels are known to be susceptible to stress corrosion cracking (SCC) [14], and the addition of more than 10% chromium is needed to reduce the susceptibility to SCC. In order to give rust resistance, chromium of more than 12% must be added [15]. In order to give corrosion resistance against a strong acid, chromium of more than 15% will be necessary [16]. Given the intended application of these steels in large cryogenic structures, rust resistance is desirable to maintain the alloy surface during construction. The suitable region for the cryogenic steels is drawn in the Fe-Mn-Cr phase diagram in Fig. 15. Alloy strength is achieved by addition of nitrogen. In order to obtain a strength of more than 1 GPa at 4.2 K, more than 0.20% nitrogen must be added. The carbon content must be held to a low value since the addition of carbon results in the precipitation of carbides at the grain boundaries and reduces the toughness of the alloy.

One alloy (similar to the base alloy (A) in the preliminary test) was selected in the region which is indicated in Fig. 15 and melted by vacuum induction melting. The carbon content was held to 0.024%. The tensile properties and the fracture toughness were investigated, and the influence of the processing (hot rolling, solution treatment, and cold rolling) on the above properties were clarified. The results are described in the following section.

D. The Tensile Properties and the Fracture Toughness at 4.2 K of the Selected Alloy.

The nominal alloy composition was 18Mn-5Ni-16Cr-0.02C-0.22N. Plates that were solution-treated and as-hot-rolled from 1250°C were cold-rolled to 21 mm thickness plate (30% rolling reduction) at room temperature in order to investigate the effect of cold rolling.

The tensile properties obtained at 4.2 K are summarized in Fig. 16. The yield and tensile strength increase with decreasing hot rolling temperature. The total elongation and the reduction of area are almost independent of the hot rolling condition. The as-rolled plates have high work-hardening rates and relatively large uniform elongations, but small local necking. A large increase in the yield and tensile strength results from 30% cold rolling at room temperature, more than 400 MPa at 4.2 K. The cold-worked specimens (AR + 30% cold rolling and ST + 30% cold rolling) showed a clear local necking at the fractured position.

The grain size decreases on decreasing the hot-rolling temperature, though large elongated unrecrystallized grains are mixed in the fine grains of the specimen hot rolled at 1150°C. The yield strength is plotted as a function of reciprocal root of the average grain size ($d^{-1/2}$) in Fig. 17. The yield strength of the as-rolled plates obeys the Hall-Petch relation like most common FCC metals. Therefore, the increase in the strength with decreasing hot-rolling temperature is mainly due to grain refinement.

The fracture toughness ($K_{IC}(J)$) that was calculated from the J_{IC} value is also plotted as a function of the reciprocal root of the average grain size in Fig. 17. An inverse relationship between K_{IC} and $d^{-1/2}$ was obtained for the as-rolled plates. The K_{IC} decreases rapidly with decreasing grain size. Since the inverse relationship of K_{IC} and yield strength is well known, K_{IC} is plotted as a function of the yield strength in Fig. 18. The data for the cold-rolled plates are also given in Fig. 18. The linear relationship that applies to 304N steels [16] is also included in the figure. The slope of the strength-toughness relationship of the as-rolled plates is steeper than that of 304N steels. The deterioration in toughness on decreasing the hot-rolling temperature is higher than expected from the increase in strength. Figure 19 shows the fractography of the as-rolled plate specimens fractured at 4.2 K. Relatively large ductile dimples are observed on the fracture surface of the 1250°C hot-rolled plate (Fig. 19a). The ductile dimples are less clear in samples rolled at lower temperature (Fig. 19 b and c). Figure 20 shows the fracture surfaces of the cold-rolled plates. Although the toughness of the cold-rolled material decreases with an increase in yield strength, the decrease in the toughness is comparable to that of 304N. Fine, clear dimples are visisble on the fracture surfaces as shown in Fig. 20. The as-rolled plate showed little necking prior to fracture in spite of the large uniform elongation that is due to the high work-hardening rate. About 20% hexagonal ε phase was detected on the fracture surface of the 1250°C hot-rolled plate. The formation of the ε phase during deformation raises the work-hardening rate as pointed out by Sato, et al. [14] and, accordingly, restricts local necking.

It is clear from Fig. 18 that the selected alloy of high manganese and high chromium has a 4 K strength and combination superior to that of 304N steel. Recently, Yoshida, et al. have proposed [19] the strength and toughness values that will be required for the structural material of the next fusion reactor. The region proposed by Yoshida, et al. (σy 1200 MPa and K_{IC} 200 MPa m) is indicated in the figure; the 1200°C hot-rolled plate satisfies the requirement.

The fatigue crack growth rates of this alloy were measured at 77 and 4.2 K and found to be substantially below those of 304LN steels [20,21].

IV. CONCLUSION

The present investigation of high manganese stainless steels yields several important results:

1. Alloys containing delta ferrite show a pronounced loss of toughness after solution treatment plus aging. Delta ferrites are formed in the alloys containing high manganese, high chromium or low nickel. The boundary of the delta ferrite formation in the Fe-Mn-Cr system shifts to the

manganese behaves as a delta-ferrite-stabilizing element. The delta ferrite transforms to brittle sigma phase on agining and reduces the toughness significantly.

2. Alloys containing carbon in substitution for nitrogen also show a loss of the ductility and toughness after solution treatment plus aging. This loss in properties is due to grain boundary precipitation of $M_{23}\tau_6$ type carbide.

3. The fracture toughness at 4.2 K was measured on an alloy of 18Mn-5Ni-16Cr-0.02C-0.22N which was selected to avoid delta ferrite, minimize carbon contenet, and achieve a fully stainless teel. The grain refinement obtained by decreasing the hot-rolling temperature reduces the toughness more rapidly than that expected by the associated increase in the yield strength. A small amount of cold rolling results in an increase in the local necking and is more effective to increase the strength without a rapid loss of the toughness. The selected alloy was found to have a significant potential as a new high strength structure material in the superconducting magnet system for the future fusion reactor.

ACKNOWLEDGEMENTS

This work is supprted by the Director, Office of Energy Research, Office of Basic Energy Science, Material Science Division of the U.S. Department of Energy under contract #DE-AC03-76SF00098.

REFERENCES

1. D.T. Reed and R.P. Reed: Materials Studies for Magnetic Fusion Energy Applications at Low Temperature-II, NBS1R 79-1609, 1979, p. 81.

2. H. Yoshimura, N. Yamada, H. Yada, H. Honma and T. Ito: Trans. ISIJ, 1979, vol. 16, p. 120.

3. R. Miura, K. Onishi, K. Yoshida and Y. Takahasi: Tetsu-to-Havane, vol. 68, 1982, S490.

4. J. Charles, A. Berghezan and A. Lutts: Proc. of ICMC, Kobe, Japan, Butterworth, 1982, p. 120.

5. T. Horiuchi, R. Ogawa, M. Shimada, S. Tone and Y. Kasamatsu: Adv. in Cryogenic Eng. Mat., 1982, vol. 28, p. 93.

6. T. Horiuchi, M. Shimada, T. Fukutsuka and S. Tokuda: Proc. 5th Int. Cryogenic Eng. Conf., IPS Sc. and Tech. Press, London, 1974, p. 339.

7. Y. Ohmori and Y. Maehara: Trans. ISIJ, 1984, vol. 24, p. 60.

8. J. Barcik and B. Brzycka: Metal Science, 1983, vol. 17, p. 256.

9. A.L. Schaefler: Metal Progress, 1949, vol. 56, p. 680.

10. DeLong, G. Ostrom and E. Szumachowdki: Welding J., 1956, vol. 35, p. 526S.

11. O.H. Henry, M.A. Cordovi and G.J. Fisher: Welding J., 1955, vol. 34, p. 735.

12. F.C. Hull: Welding J., 1973, vol. 52, p. 1938.

13. Y. Takahasi, K. Yoshida, M. Shimada, E. Tada, R. Miura and S. Shimamoto: Adv. in Cryogenic Eng. Mat., 1982, vol. 28, p. 73.

14. K. Fujiwara, k. Sugie, T. Nakayama and K. Shimogori: Boshoku Gijutsu (Corrosion Eng.), vol. 33, 1984, p. 266.

15. H.L. Maxwell: The Corrosion Handbook, H.H. Uhlig (ed.), John Wiley β Sons, NY, 1948, p. 150.

16. R. Ranks: The Corrosion Handbook, H.H. Uhlig (ed.), John Wiley β Sons, NY, 1948, p. 189.

17. R.L. Tobler, D.T. Reed and R.P. Reed: Materials Studies for Magnetic Fusion Energy Applications at Low Temperatures-IV NBS1R-1645, 1981, p. 37.

18. A. Sato, K. Soma and T. Mori: Acta Metall., 1983, vol. 30, p. 10.

19. K. Yoshida, H. Nagajima, K. Koizumi, M. Shimada, Y. Takahasi, E. Tada, H. Tsuji and S. Shimamoto: Austenitic Steels at Low Temperatures, R. Reed and T. Horiuchi (eds.), Plenum Press, NY, 1983, p. 29.

20. R. Ogawa and J.W. Morris, Jr.: Adv. in Cryogenic Eng. Mat., vol. 30, 1984, p. 177.

21. R. Ogawa and J.W. Morris, Jr.: Fatigue at Low Temperatures, ASTM STP857, 1985, p. 47.

Table 4 Chemical composition of delta and sigma phases of 29Mn-1Ni-16Cr steel (at.%) by EPMA analysis

	Solution Treatment (1050 C x 30min-WQ)		S.T. + Aging (S.T. + 660 C x 30 min)	
	Matrix at.%	Delta ferrite at.%	Matrix at.%	Sigma phase at.%
Cr	16.8	24.0	16.7	23.9
Mn	29.3	25.5	29.2	25.8
Fe	52.8	50.0	53.1	49.6
Ni	1.1	0.6	1.1	0.6

Table 3 Permeability measurement of high Mn stainless steels

	Solution Treat. 1050°C x 30 min→WQ	St+Annealing 660°C x 45 min	As Rolled
28Mn-5Ni-16Cr	$1.02 < \mu < 1.05$	< 1.01	< 1.01
18Mn-5Ni-18Cr	$1.02 < \mu < 1.05$	< 1.01	$1.01 < \mu < 1.02$
18Mn-1Ni-16Cr	$1.02 < \mu < 1.05$	< 1.01	$1.01 < \mu < 1.02$
22Mn-1Ni-16Cr	$1.05 < \mu < 1.10$(0.4)	< 1.01	$1.01 < \mu < 1.02$
29Mn-1Ni-16Cr	$1.60 < \mu < 2.00$(4.6)	< 1.01	< 1.01

C ∿ 0.03%
N ∿ 0.25%

( ) ferrite number by Magne Gauge

Table 2 Chemical compositions of 18Mn-5Ni-16Cr-C-N steel

	C	Si	Mn	Ni	Cr	P	S	N	C+N
18Mn-5Ni -16Cr	0.024	0.53	17.99	4.97	16.28	0.004	0.01	0.216	0.240

Table 1 Chemical compositions of high Mn stainless steels

	C	Si	Mn	Ni	Cr	P	S	N	C+N
A	0.031	0.11	18.64	5.06	16.11	0.001	0.01	0.261	0.292
B	0.037	0.12	18.09	5.08	18.10	0.001	0.01	0.243	0.280
C	0.032	0.10	18.18	7.12	16.19	0.001	0.01	0.251	0.283
D	0.033	0.10	18.16	3.11	16.30	0.001	0.01	0.231	0.264
E	0.034	0.10	18.16	1.07	16.53	0.001	0.01	0.241	0.275
F	0.031	0.10	15.01	5.08	16.23	0.001	0.01	0.237	0.272
G	0.032	0.11	20.00	5.10	15.94	0.001	0.01	0.246	0.278
H	0.033	0.10	22.00	5.12	15.94	0.001	0.01	0.245	0.278
I	0.037	0.10	28.60	5.12	15.98	0.001	0.01	0.247	0.284
J	0.100	0.09	18.80	5.09	16.02	0.001	0.01	0.177	0.277
K	0.160	0.10	18.80	5.00	16.02	0.001	0.01	0.122	0.282
L	0.036	0.09	22.30	5.09	12.23	0.001	0.01	0.225	0.261
M	0.035	0.09	28.60	1.04	16.20	0.001	0.01	0.255	0.290
N	0.032	0.10	22.30	1.11	15.98	0.002	0.01	0.251	0.283

Figure Captions

Fig. 1. Influence of Mn on the tensile properties of Fe-XMn-5Ni-16Cr-0.03C-0.25N steels at 4.2 K.

Fig. 2. Influence of Mn on the tensile properties of Fe-XMn-1Ni-16Cr-0.03C-0.25N steels at 4.2 K.

Fig. 3. Influence of Cr on the tensile properties of Fe-(18, 22%)Mn-5Ni-XCr-0.03C-0.25N steels at 4.2 K.

Fig. 4. Influence of Ni on the tensile properties of Fe-18Mn-XNi-16Cr-0.03C-0.25N steels at 4.2 K.

Fig. 5. Influence of Mn on the Charpy impact values of Fe-Xmn-(1,5%)Ni-16Cr-0.03C-0.25N steels at 77 K.

Fig. 6. Influence of Cr (a) and Ni (b) on the Charpy impact values of Fe-(18,22%)Mn-Cr-Ni-0.03C-0.25N steels at 77 K.

Fig. 7. The fracture surface of the Charpy impact specimens fractured at 77 K, a) 18Mn-1Ni-16Cr, b) 29Mn-1Ni-16Cr steels.

Fig. 8. The optical micrographs of the delta ferrite a) and the sigma phase b) of 20Mn-1Ni-16Cr steel.

Fig. 9. The micrographs of the sigma phase in 29Mn-1Ni-16Cr steel.

Fig. 10. The phase diagram for delta ferrite on Fe-Mn-Cr system.

Fig. 11. Influence of C on the tensile properties of 18Mn-5Ni-16Cr-C-N steels at 4.2 K.

Fig. 12. Influence of C on the Charpy impact values of 18Mn-5Ni-16Cr-C-N steels at 77 K.

Fig. 13. The fracture surface of the notched specimen of 18Mn-5Ni-16Cr-0.16C-0.122N steel fractured at 77 K in the specimen chamber of an Auger Electron Spectroscope.

Fig. 14. The grain boundary precipitates of the aged plate of 18Mn-5Ni-16Cr-0.16C-0.122N steel.

Fig. 15. The suitable region for a cryogenic steel with rust resistance in an Fe-Mn-Cr system.

Fig. 16. The tensile properties of 18Mn-5Ni-16Cr-0.024C-0.216N steel at 4.2 K.

Fig. 17. The yield strength and the $K_{IC}(J)$ values of 18Mn-5Ni-16Cr-0.024C-0.216N steel at 4.2 K are plotted as a function of reciprocal root of the average grain size ($d^{-1/2}$).

Fig. 18. The relationship between the yield strength and $K_{IC}(J)$ values of 18mn-5Ni-16Cr-0.024C-0.216N in comparison with the data of 304N steels.

Fig. 19. The fracture surfaces of the as-rolled plates of 18Mn-5Ni-16Cr-0.024C-0.216N steel, a) 1250°C, b) 1200°C, c) 1150°C.

Fig. 20. The fracture surfaces of the cold-rolled plate of 28Mn-5Ni-16Cr-0.024C-0.216N steel, a) 30% cold rolled after solution treatment, b) 30% cold rolled after hot rolling at 1250°C.

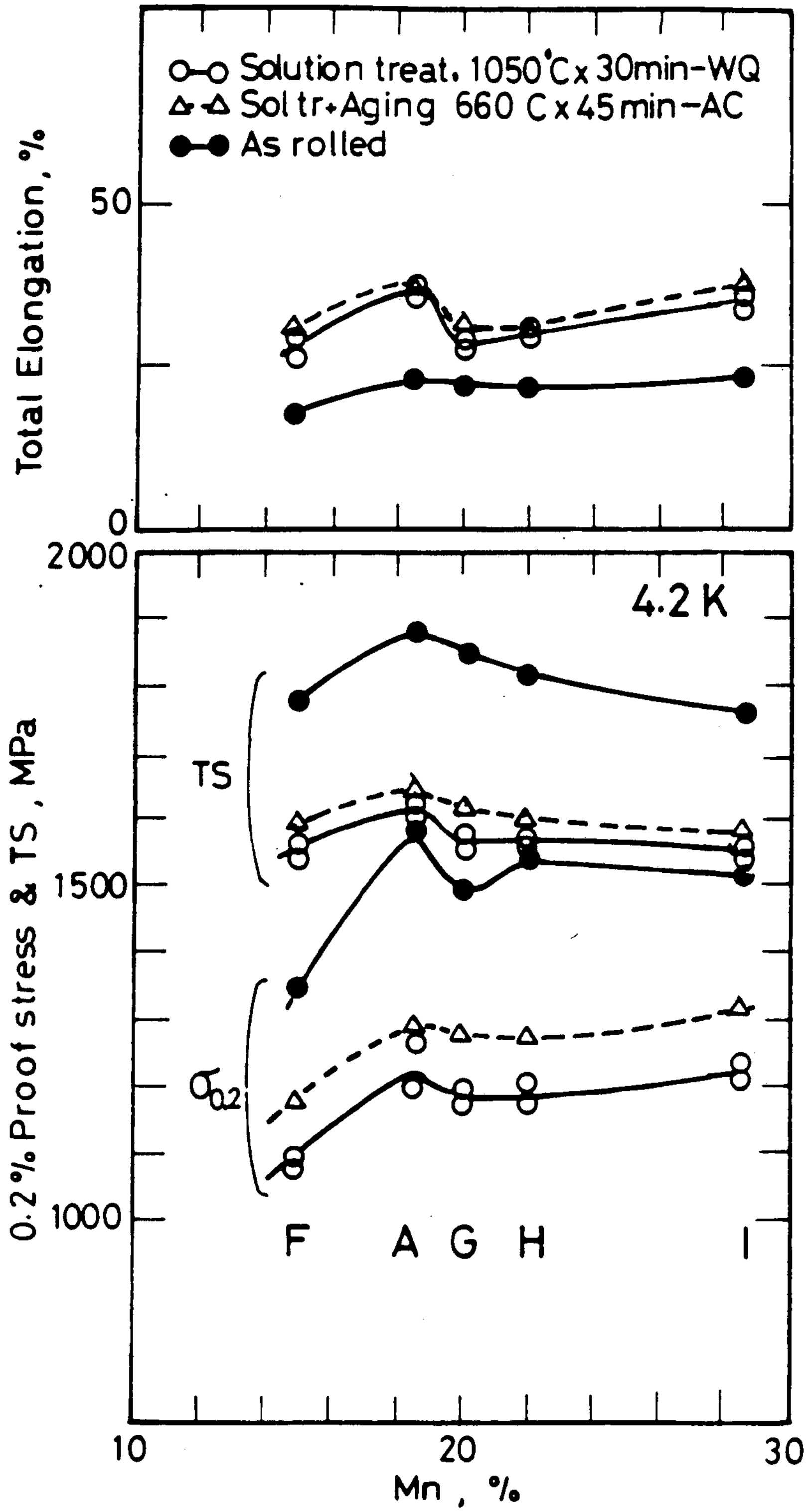

XBL 868-2838

Fig. 1

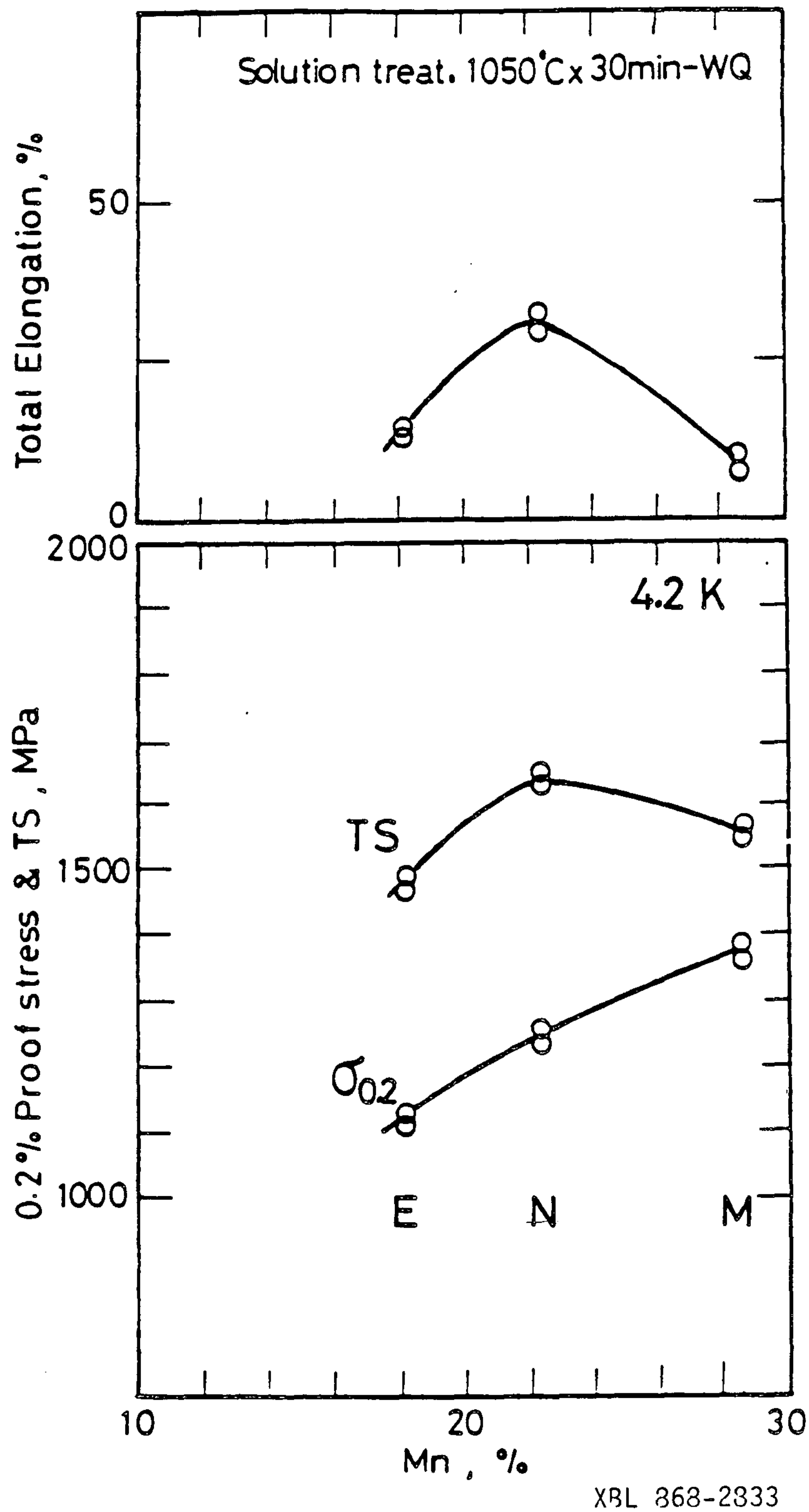

Solution treat. 1050°C x 30min-WQ
Total Elongation, %
50
0
2000
4.2 K
0.2% Proof stress & TS, MPa
TS
1500
σ0.2
1000
E
N
M
10
20
30
Mn, %
XBL 868-2333

Fig. 2

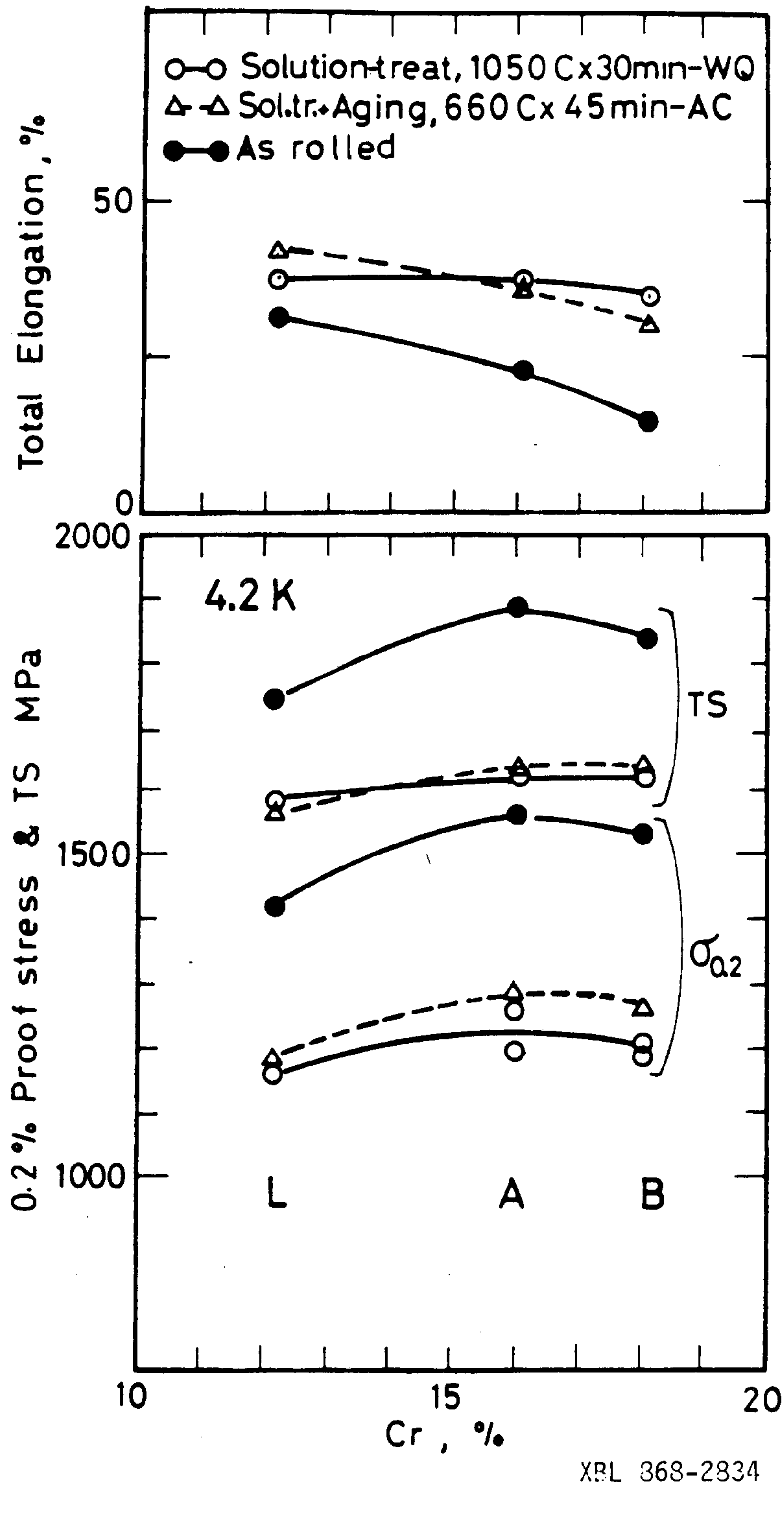

Solution-treat, 1050 Cx30min-WQ
Sol.tr.+Aging, 660 Cx 45min-AC
As rolled
Total Elongation, %
50
0
2000
4.2 K
TS
1500
$\sigma_{0.2}$
0.2 % Proof stress & TS MPa
1000
L
A
B
10
15
20
Cr, %
XBL 868-2834

Fig. 3

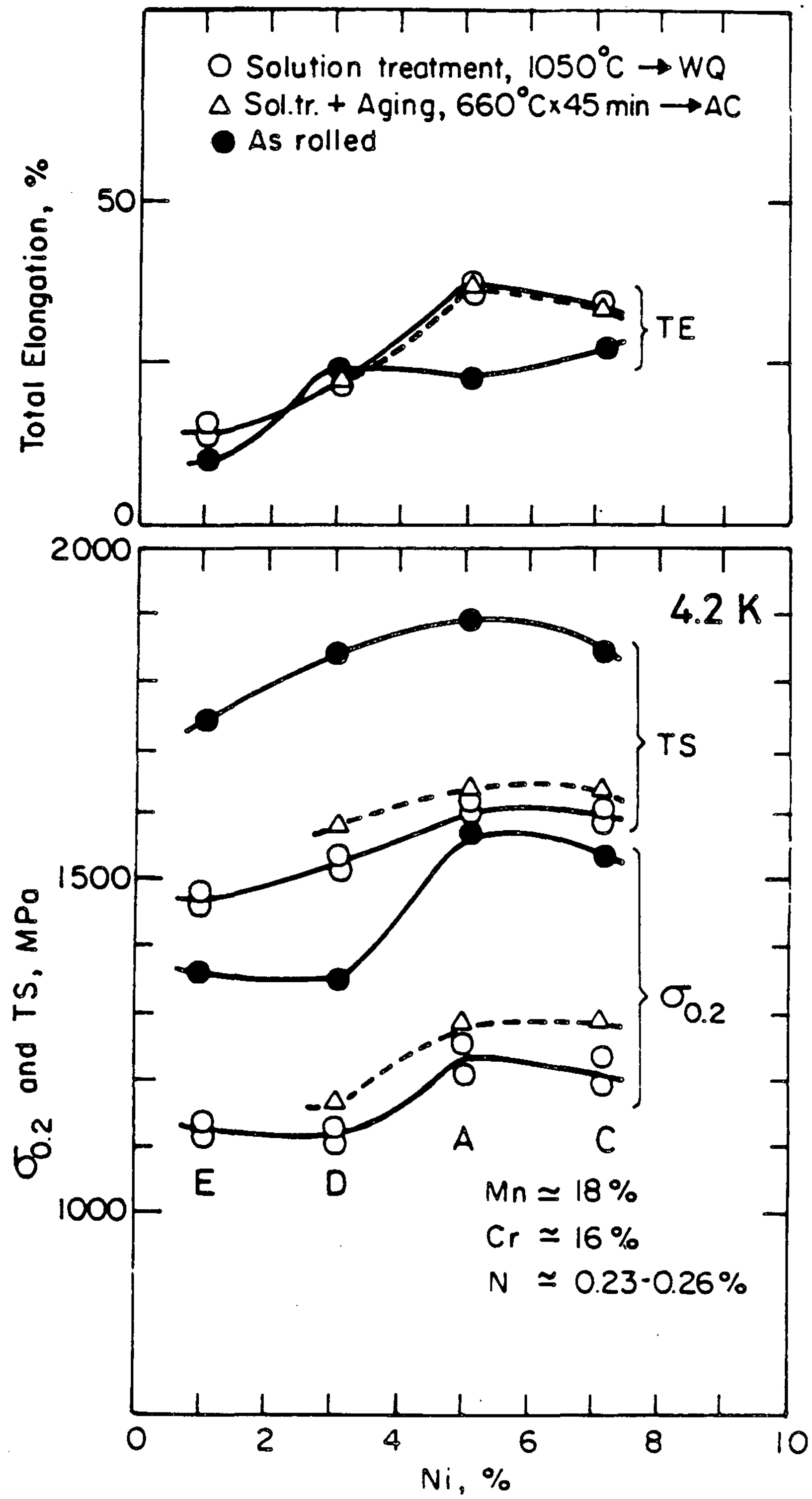

Fig. 4

XBL 868-2835

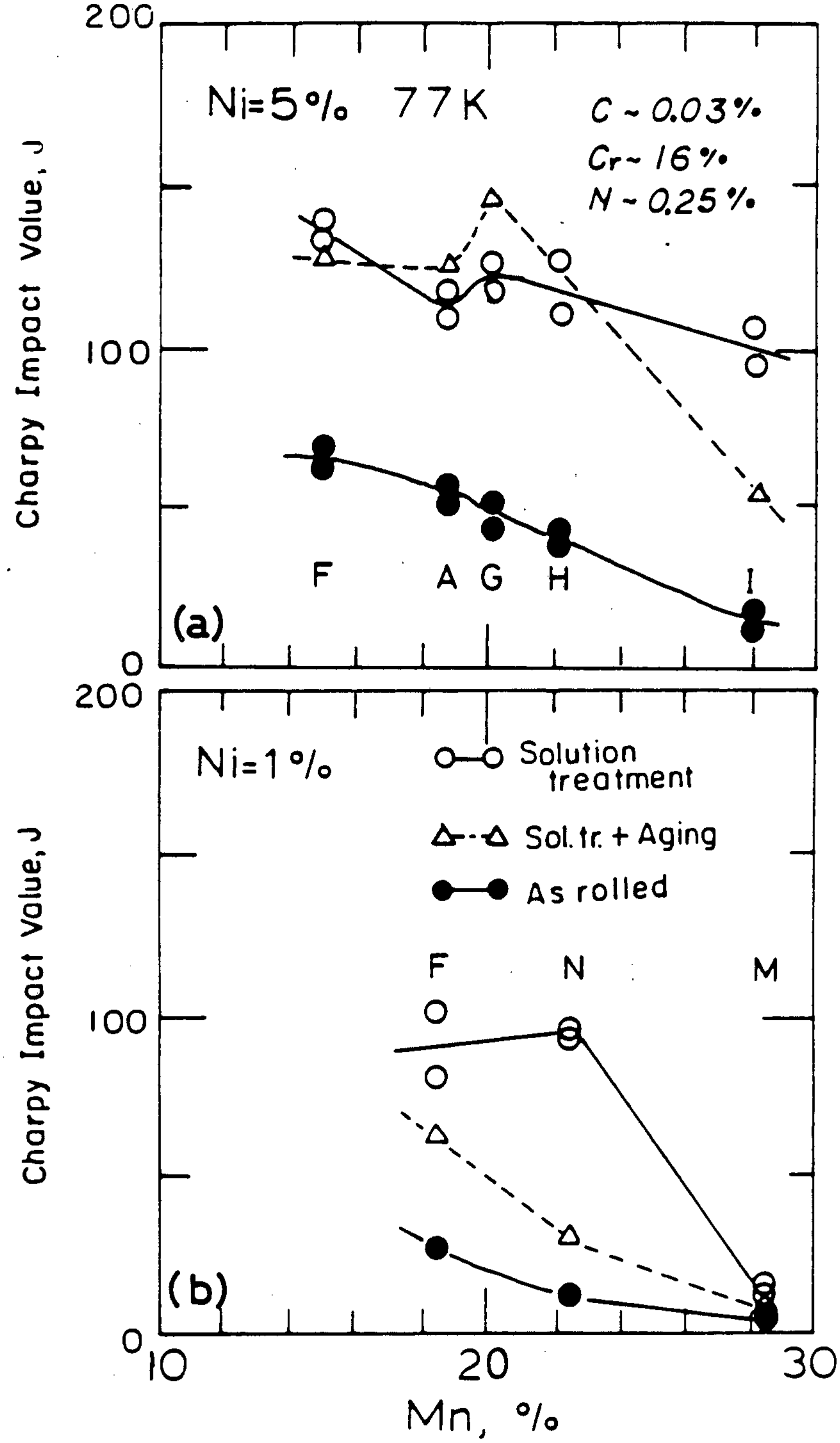

Fig. 5

XBL 868-2836

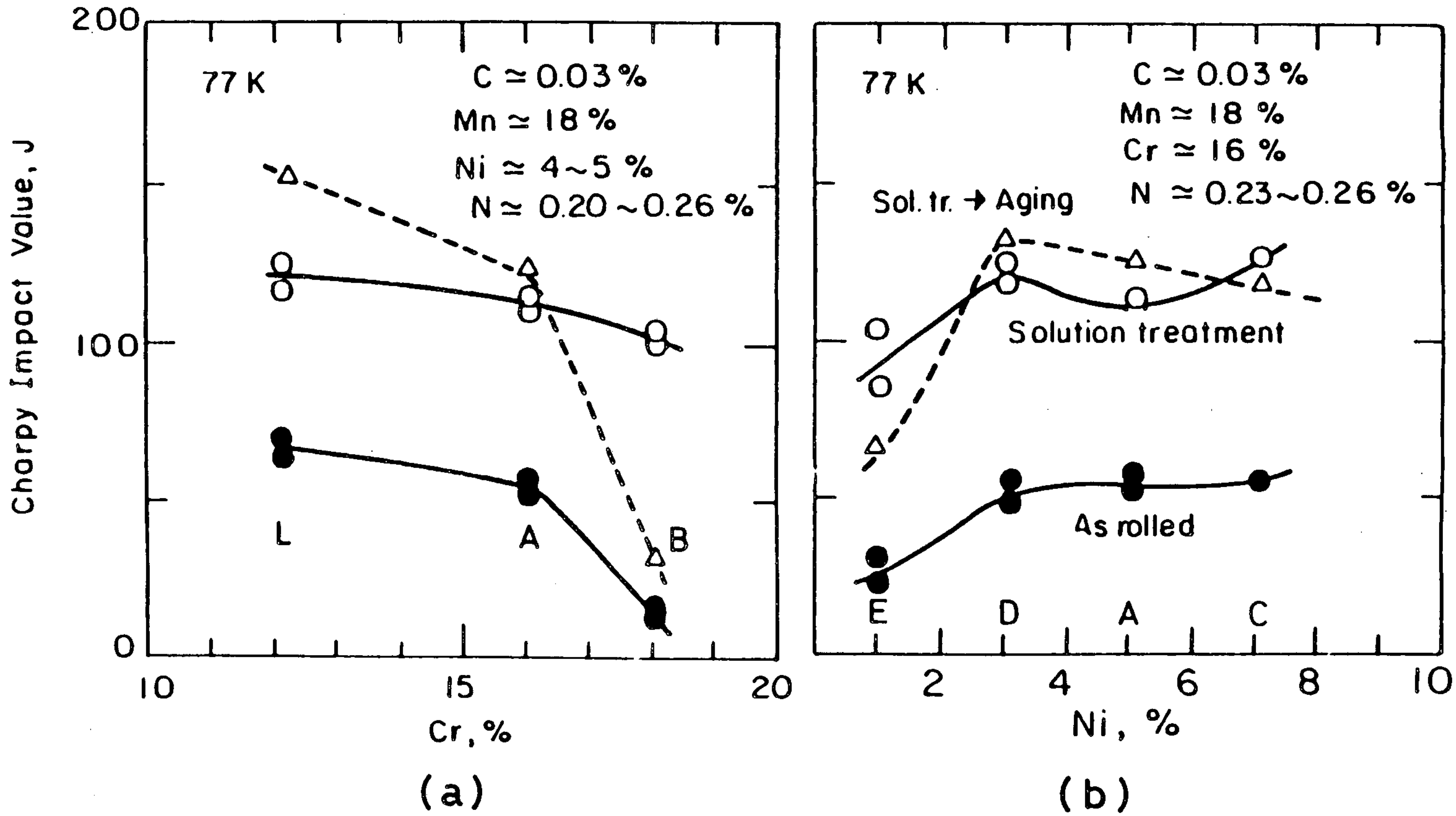

XBL 868-2837

Fig 6

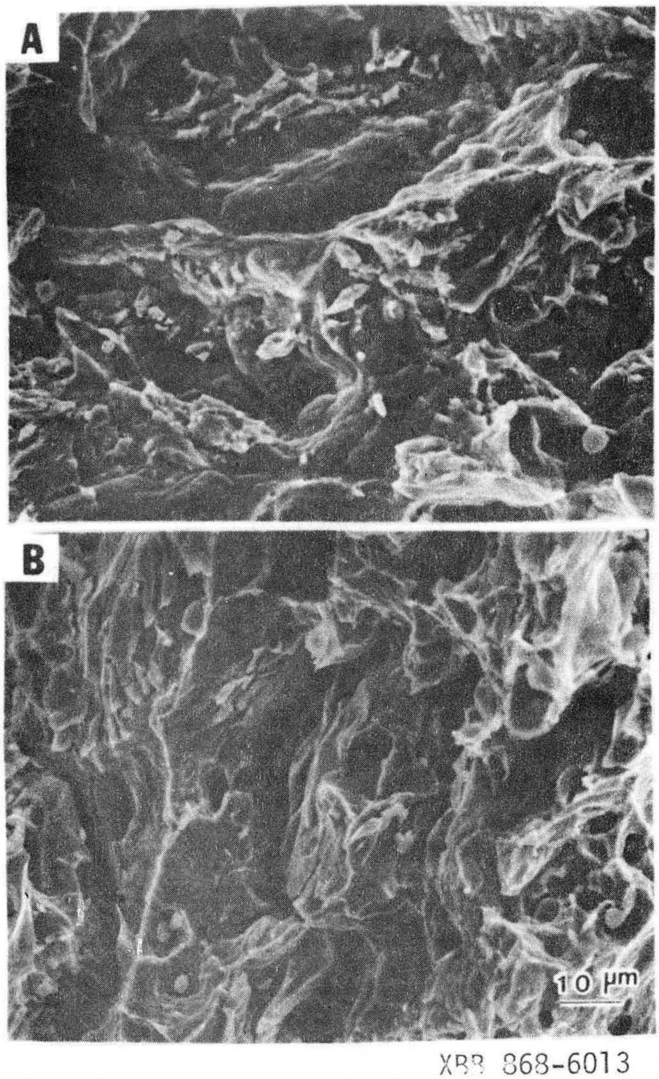

XBB 868-6013

Fig. 7

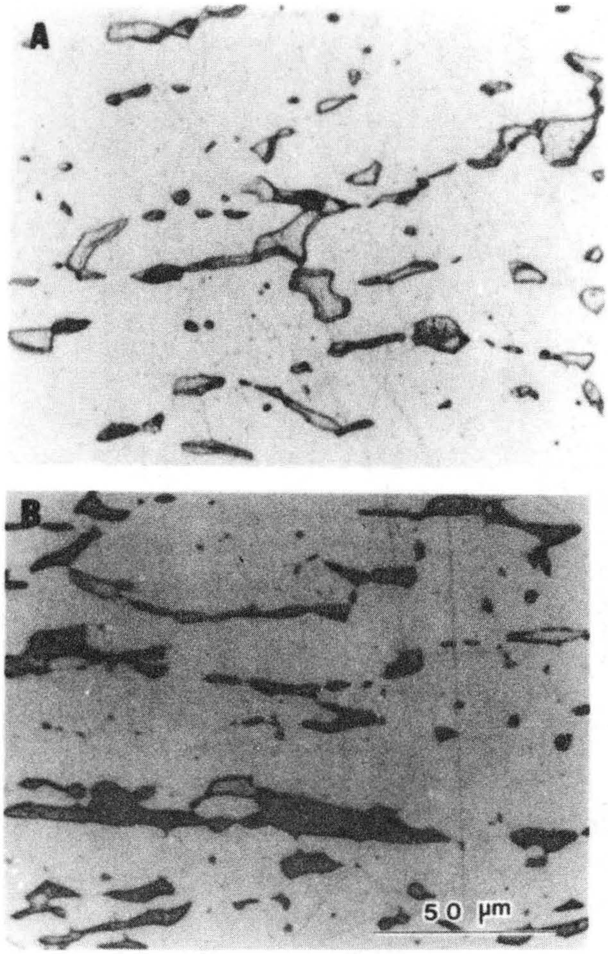

XBB 868-6014

Fig. 8

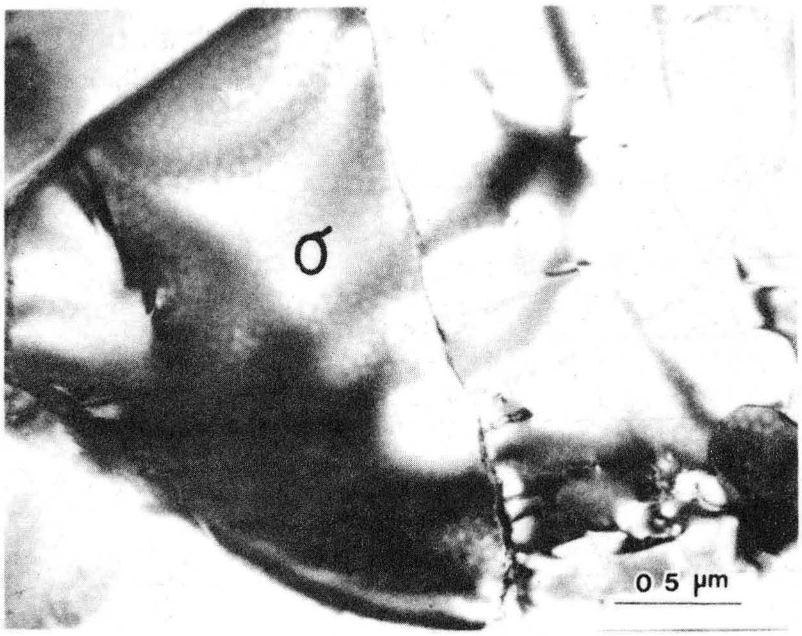

XBB 868-6015

Fig. 9

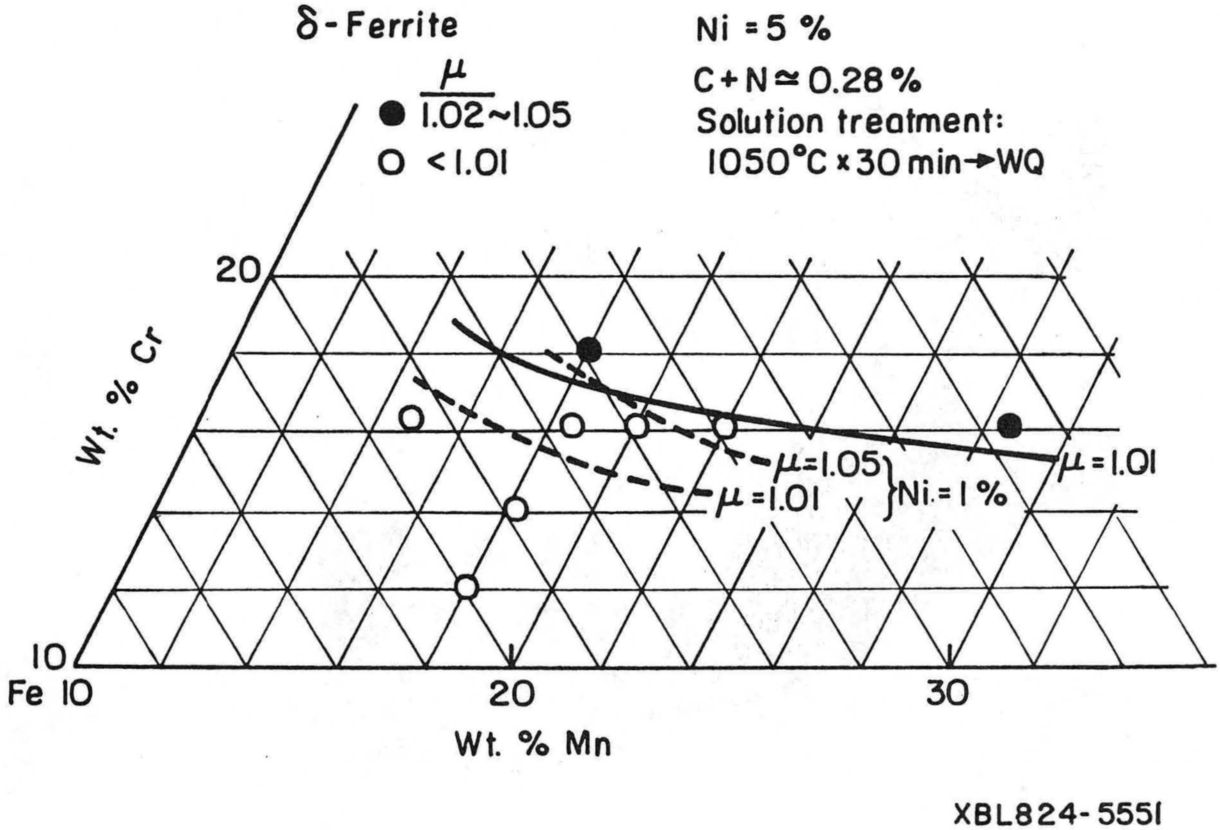

δ-Ferrite
μ
1.02~1.05
<1.01
Ni = 5 %
C + N ≃ 0.28 %
Solution treatment:
1050°C × 30 min → WQ
20
Wt. % Cr
μ=1.05
μ=1.01
Ni = 1 %
μ = 1.01
10
Fe 10
20
30
Wt. % Mn
XBL824-5551

Fig. 10

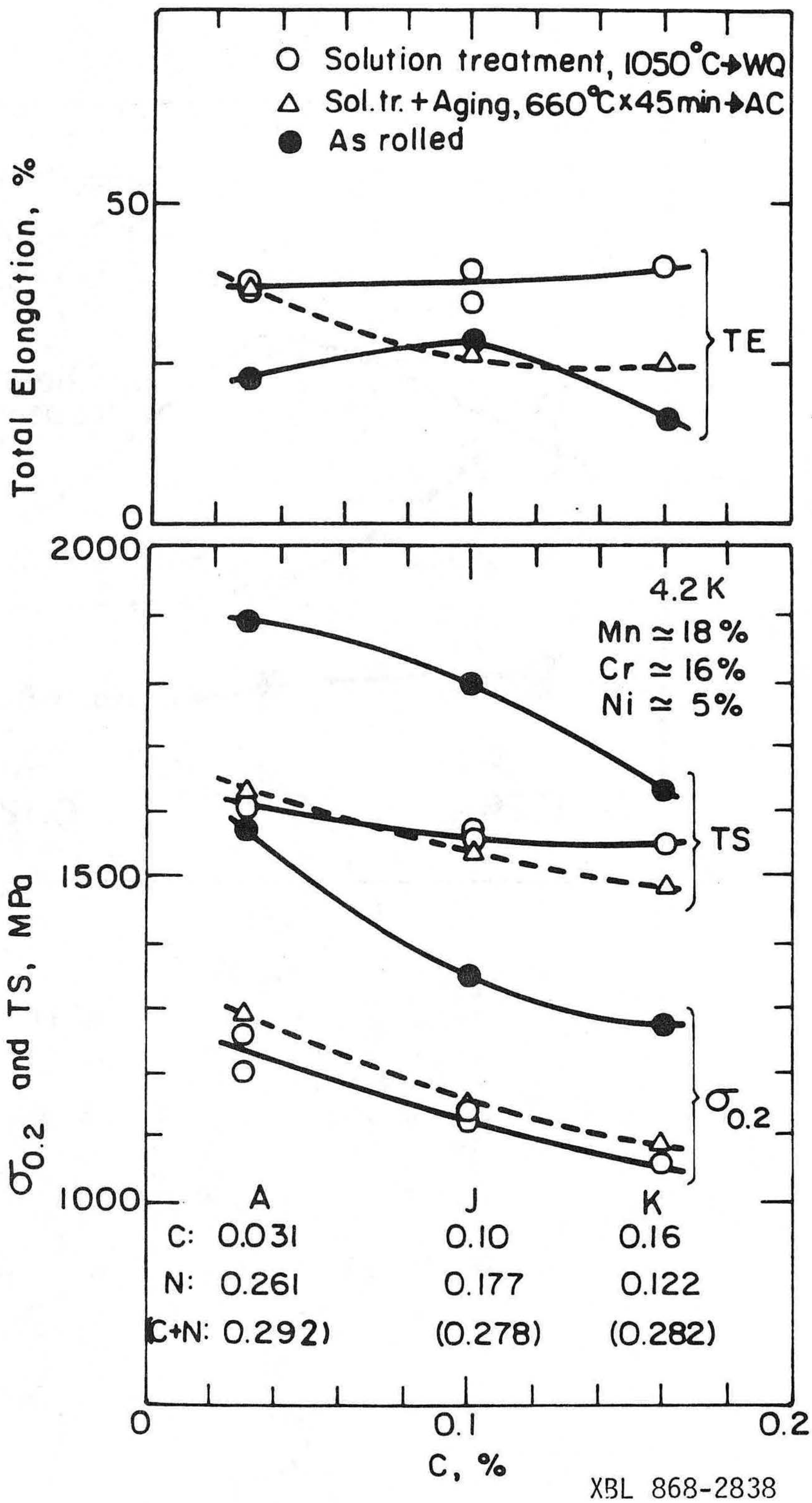

Solution treatment, 1050°C→WQ
Sol. tr. + Aging, 660°C×45min→AC
As rolled
Total Elongation, %
50
0
TE
2000
1500
1000
4.2 K
Mn ≃ 18 %
Cr ≃ 16%
Ni ≃ 5%
TS
σ0.2
σ0.2 and TS, MPa
A
J
K
C: 0.031
0.10
0.16
N: 0.261
0.177
0.122
(C+N: 0.292)
(0.278)
(0.282)
0
0.1
0.2
C, %
XBL 868-2838

Fig. 11

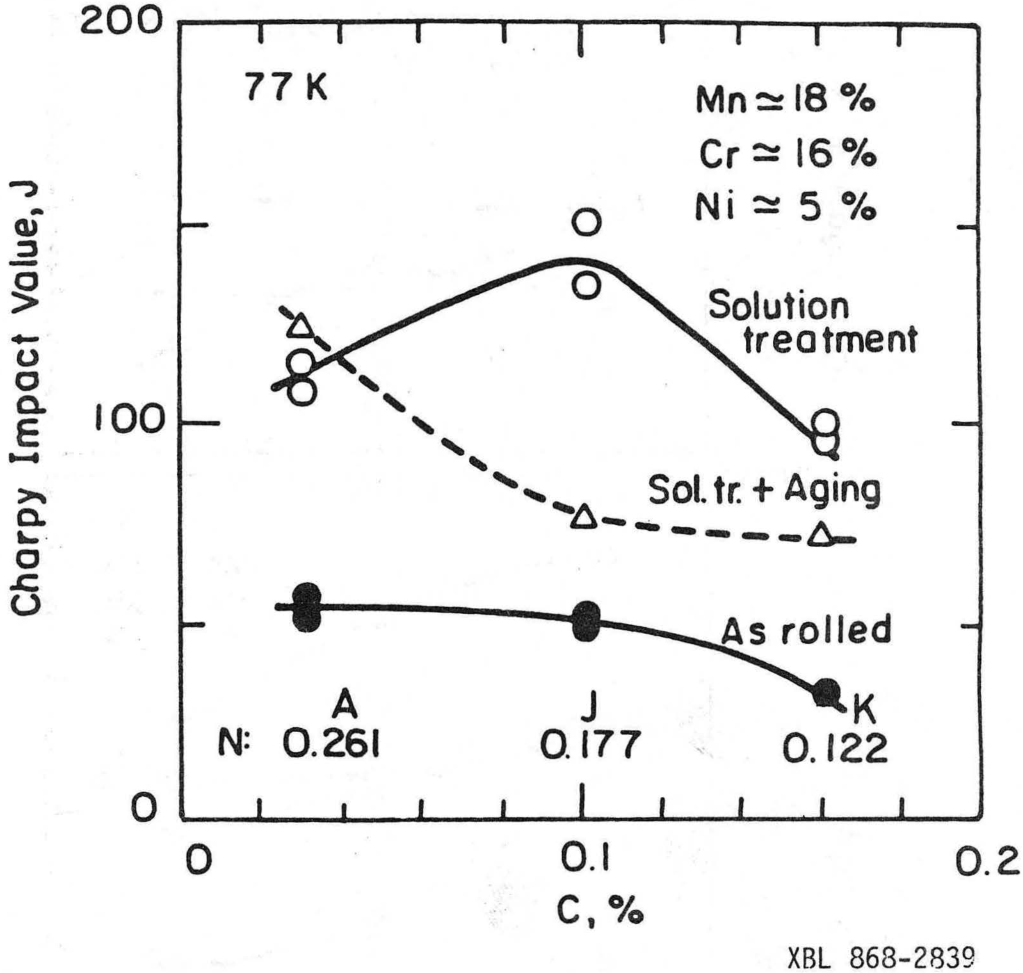

200
100
0
77 K
Mn ≃ 18 %
Cr ≃ 16 %
Ni ≃ 5 %
Solution treatment
Sol. tr. + Aging
As rolled
A
J
K
N: 0.261
0.177
0.122
Charpy Impact Value, J
0
0.1
0.2
C, %
XBL 868-2839

Fig. 12

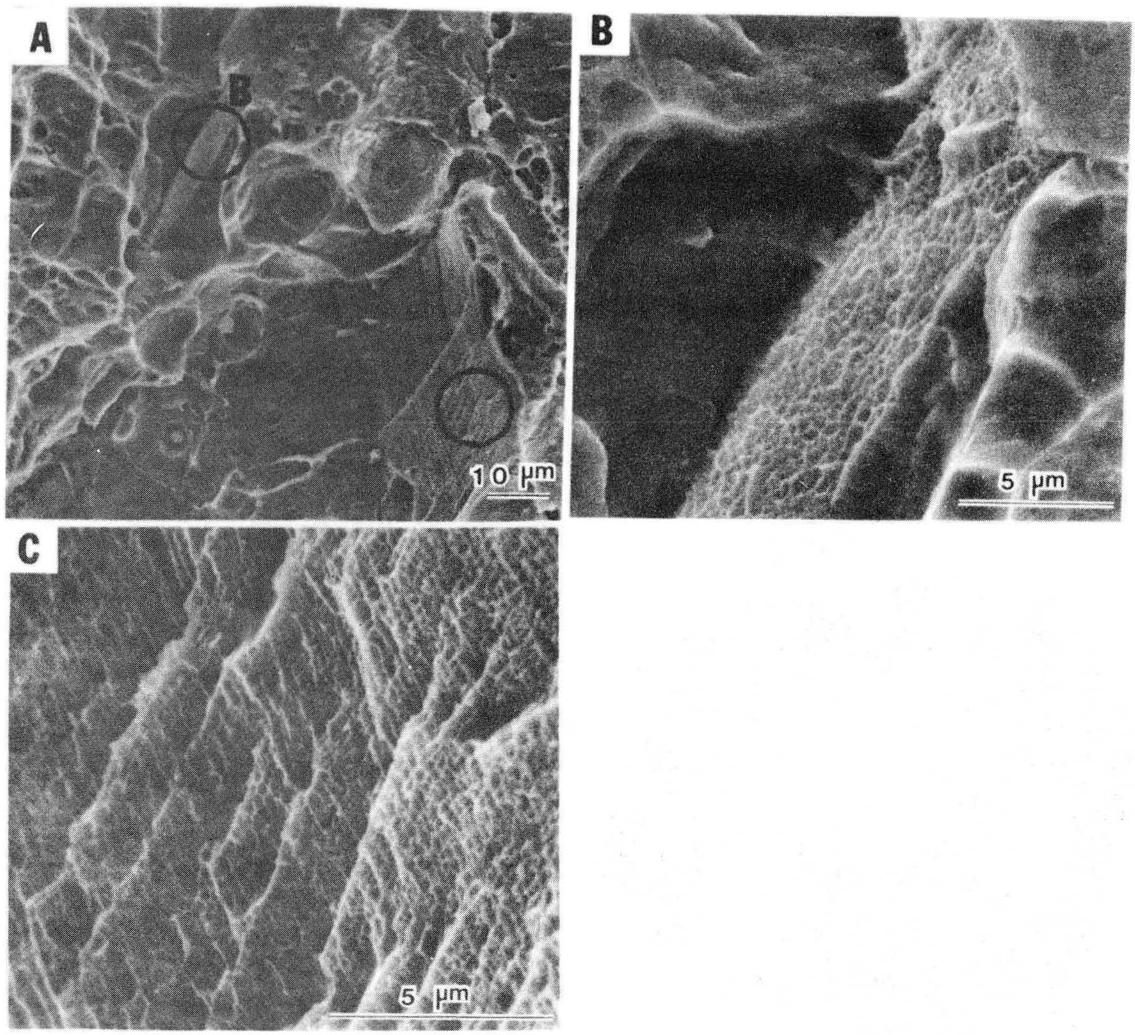

XBB 868-6016

Fig. 13

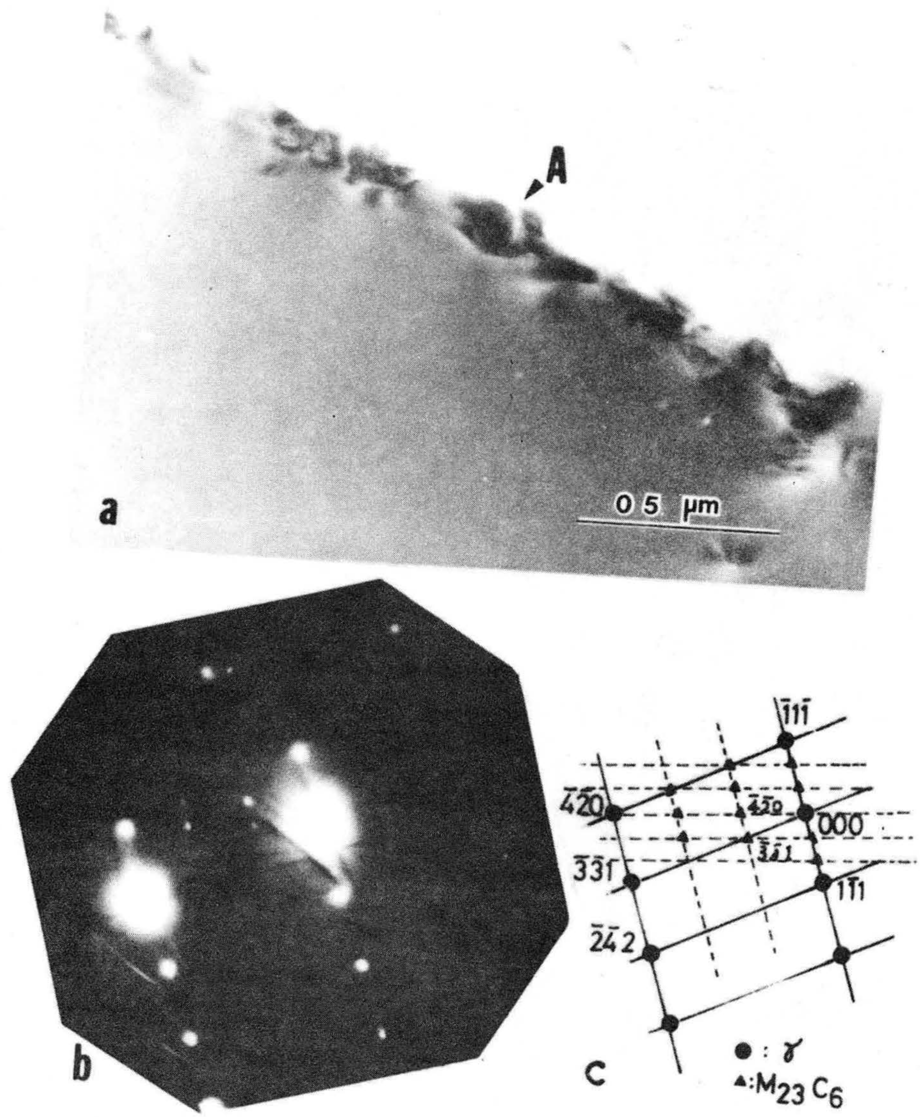

XBB 868-6017

Fig. 14

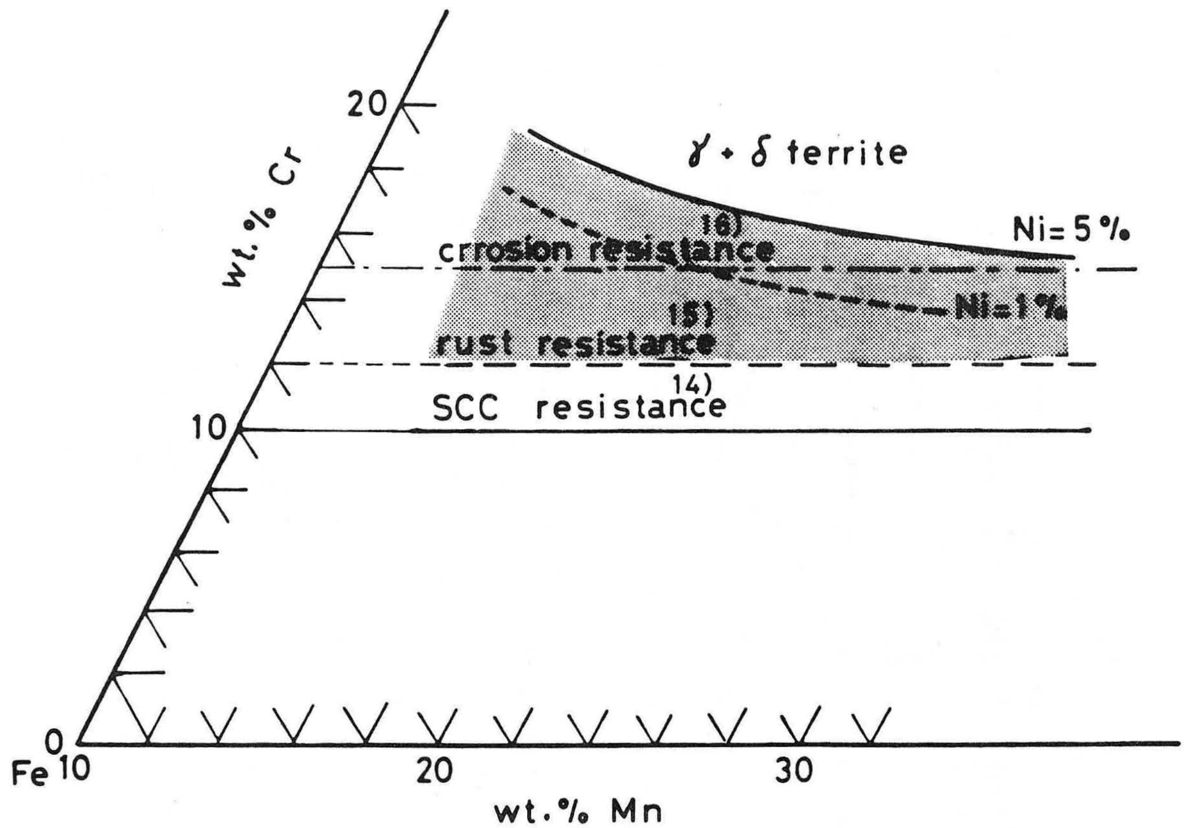

XBL 868-2840

Fig. 15

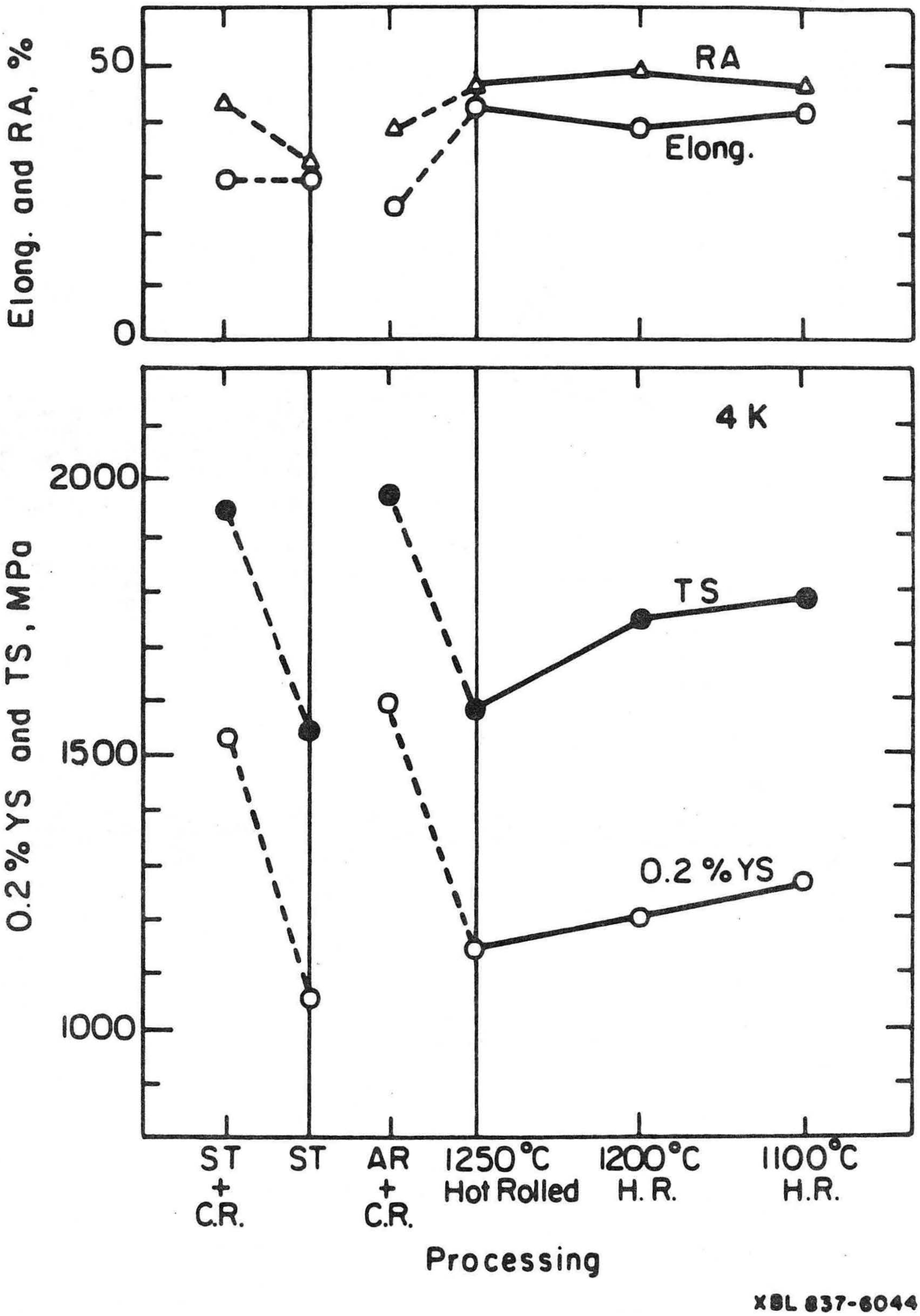
Elong. and RA, %
50
0
RA
Elong.
4 K
2000
1500
1000
0.2% YS and TS, MPa
TS
0.2 % YS
ST + C.R.
ST
AR + C.R.
1250°C Hot Rolled
1200°C H. R.
1100°C H.R.
Processing
XBL 837-6044

Fig. 16

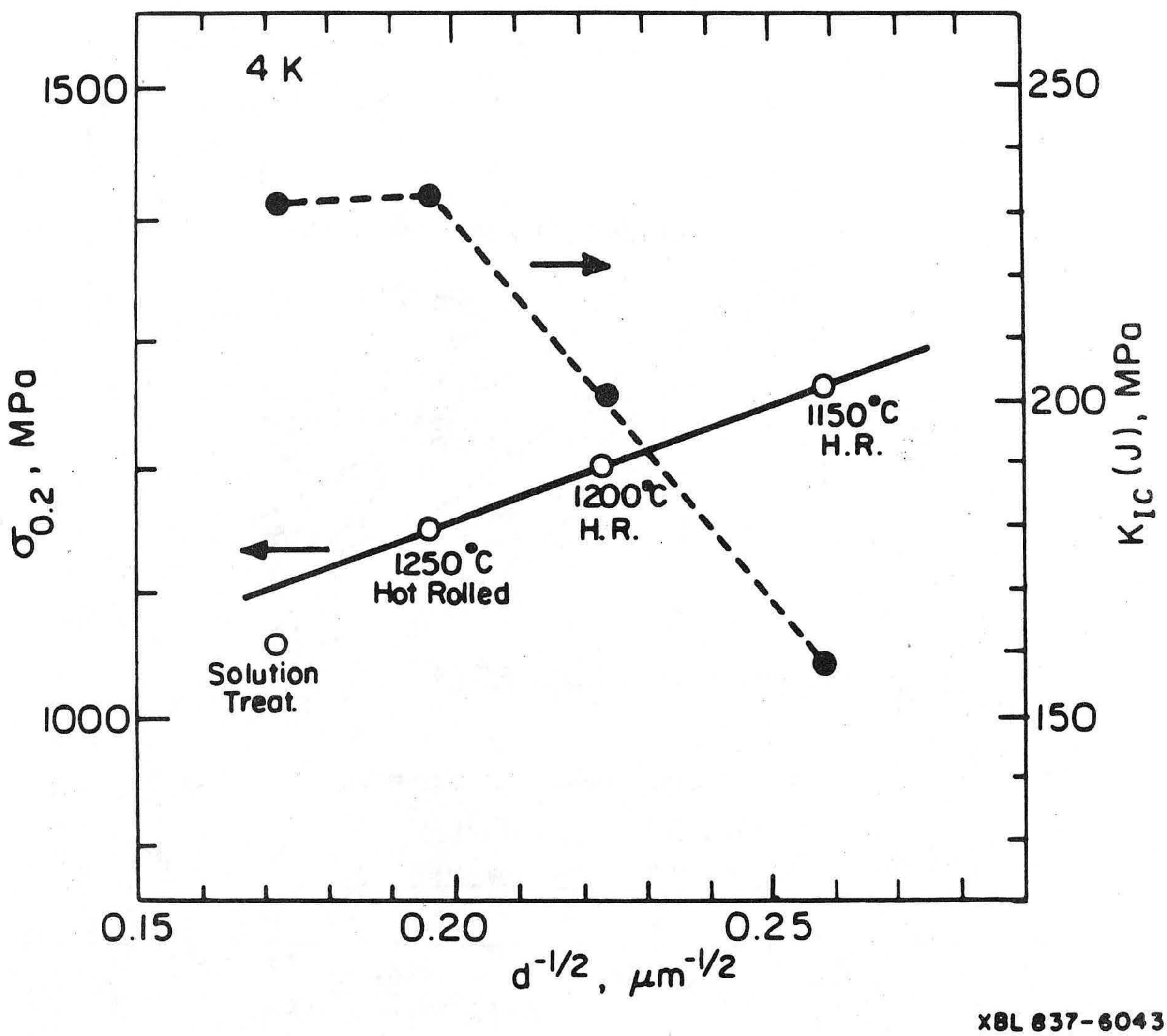
4 K
1500
1000
250
200
150
$\sigma_{0.2}$, MPa
K_{Ic} (J), MPa
1150°C
H.R.
1200°C
H.R.
1250°C
Hot Rolled
Solution
Treat.
0.15
0.20
0.25
$d^{-1/2}$, $\mu m^{-1/2}$
XBL 837-6043

Fig. 17

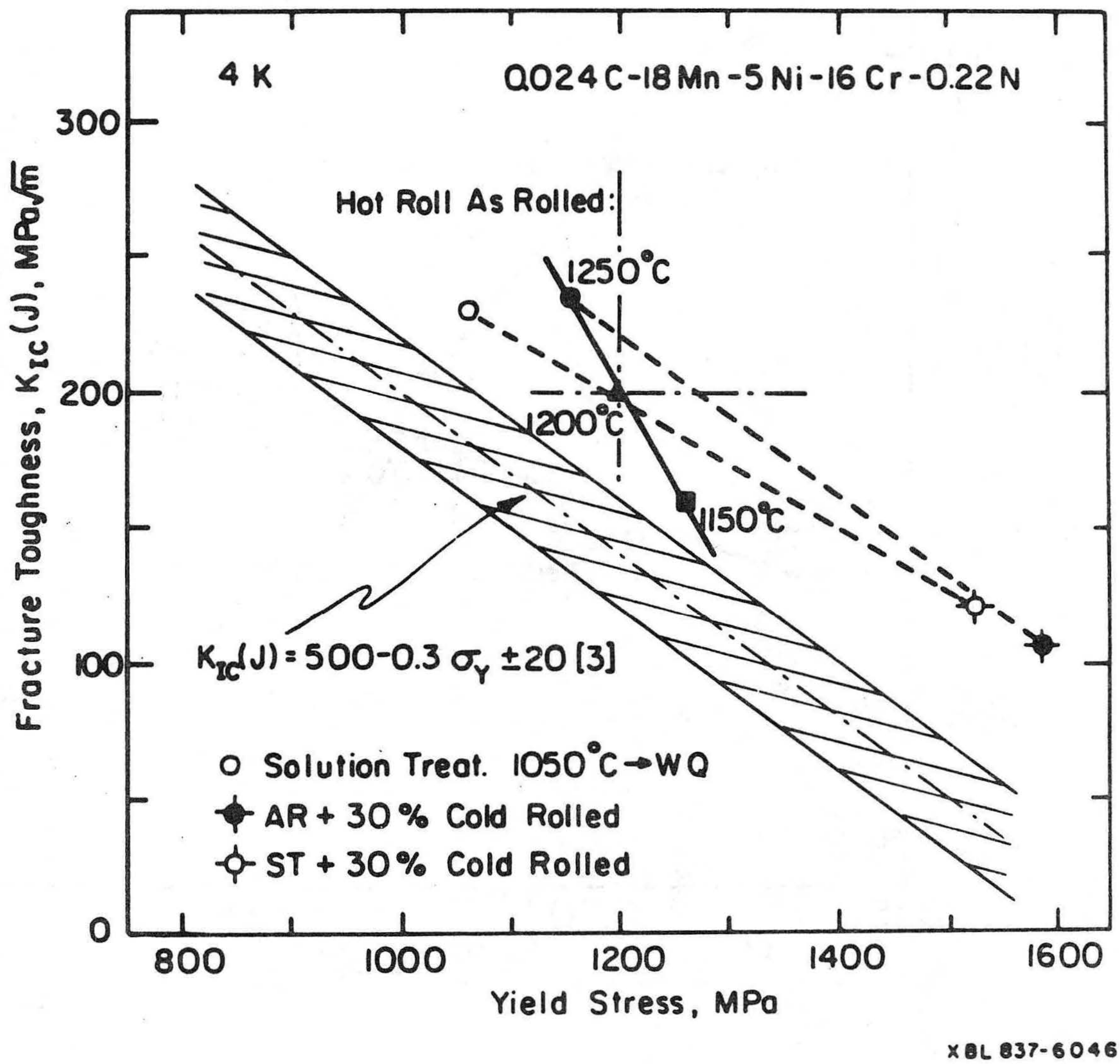
4 K
0.024 C-18 Mn-5 Ni-16 Cr-0.22 N
Hot Roll As Rolled:
1250°C
1200°C
1150°C
$K_{IC}(J) = 500 - 0.3\ \sigma_Y \pm 20$ [3]
o Solution Treat. 1050°C → WQ
AR + 30 % Cold Rolled
ST + 30 % Cold Rolled
Fracture Toughness, $K_{IC}(J)$, MPa$\sqrt{m}$
0
100
200
300
800
1000
1200
1400
1600
Yield Stress, MPa
XBL 837-6046

Fig. 18

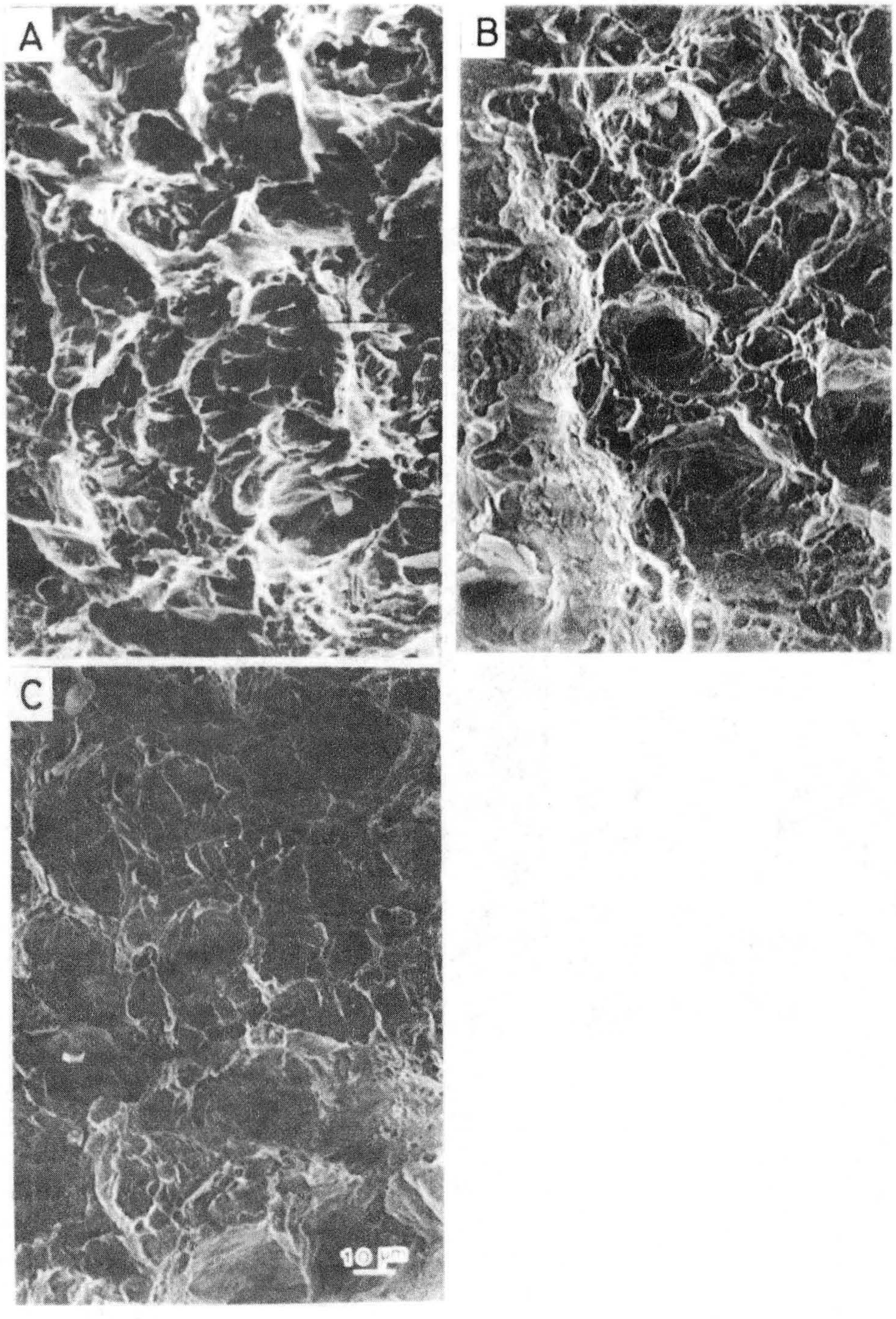

XBB 868-6018

Fig. 19

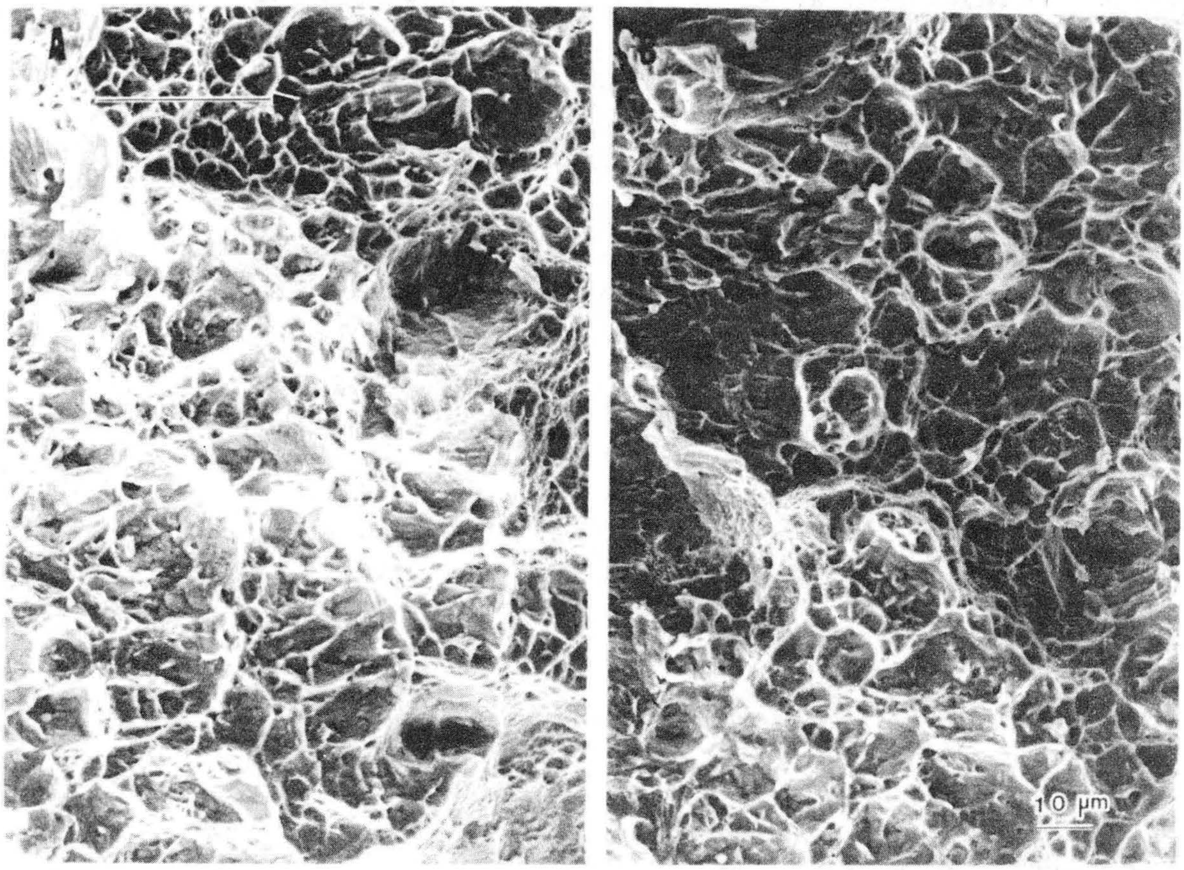

a) AR+30% Cold Rolled

b) ST+30% Cold Rolled

XBB 868-601?

Fig. 20

LAWRENCE BERKELEY LABORATORY
TECHNICAL INFORMATION DEPARTMENT
UNIVERSITY OF CALIFORNIA
BERKELEY, CALIFORNIA 94720